Hindawi
International Journal of Photoenergy
Volume 2022, Article ID 5949837, 17 pages
https://doi.org/10.1155/2022/5949837

*Research Article*

# Photoabsorption Enhancement in Synthetic-Natural Dye-Sensitized Solar Cells Using Bilayer $TiO_2$ Deposition and Separated Sensitization

**Roohollah Nakhaei**,[1] **Alireza Razeghizadeh**,[1,2] **Pejman Shabani**,[1] **Jabbar Ganji**,[1] **and Seyed Sajjad Tabatabaee**[1]

[1]*Department of Electrical Engineering, Mahshahr Branch, Islamic Azad University, Mahshahr, Iran*
[2]*Department of Physics, Payame Noor University, P.O. Box 19395-3697, Tehran, Iran*

Correspondence should be addressed to Alireza Razeghizadeh; a.razeghizadeh@gmail.com

Received 17 December 2021; Revised 26 February 2022; Accepted 18 March 2022; Published 4 April 2022

Academic Editor: Petru A. Cotfas



In this study, a new methodology is proposed for the cosensitization of dye-sensitized solar cells by synthetic and natural dyes to increase their optical absorption. Synthetic dyes are efficient but expensive. In contrast, natural dyes are cheap but have a low adsorption rate in competition with synthetic dyes. Therefore, the conventional cosensitization method which is based on dye mixing prevents complete adsorption of natural dyes. In this work, a bilayer deposition of $TiO_2$ and separated sensitization of each layer by one type of dye was performed. The N719 was used as a synthetic dye and betanin, crocin, acacetin, and indigo were used as natural dyes, which are extracted from plants inexpensively. The dyes were evaluated by UV-visible and FT-IR analyses. The results showed that a broad spectrum can be achieved due to different peaks in the photoabsorption spectra of these dyes. The bottom layer was sensitized by natural dyes while the top layer was sensitized by N719. Due to the effect of temperature on dyes, a low-temperature method based on acid-assistant sintering has been used for the top layer. The results of XRD and FESEM analyses indicated that a layer with proper crystalline phase, acceptable morphology, and good porosity can be achieved in the low-temperature process by tunning the acid concentration. The electrical properties of the fabricated solar cells were investigated by EIS analysis and J-V characteristics. The results showed that charge injection and transportation were improved via the ability of the proposed approach in separated dye adsorption. An efficiency of 3.48% was provided by the proposed method which demonstrates its better performance in comparison with the cocktail and sequential methods that showed efficiencies of 1.88% and 2.29%, respectively. The results indicated that separated sensitization of each layer can improve the dye loading leading to spectral expansion.

## 1. Introduction

Nowadays, increasing demand for sustainable, clean, and renewable energy becomes an important challenge facing humanity. For this reason, solar energy utilization as an abundant, accessible, and environmentally friendly energy source is developing rapidly [1–4]. Dye-sensitized solar cell (DSSC), first developed by O'Regan and Grätzel [5] is a good choice for this purpose due to their high environmental friendliness, low cost, easy manufacturing process, and good performance in low-light conditions [4–6]. Generally, a DSSC has several mandatory parts: a photoanode, a counter electrode, a photosensitizer (dye), and an electrolyte. The photoanode is composed of a mesoporous wide-bandgap semiconductor (e.g., $TiO_2$), which has been coated on a transparent substrate (e.g., FTO). It is responsible for absorbing the dye and transferring the excited electrons. The counterelectrode is made of a catalyst material (i.e., platinum or carbon) to inject electrons into the electrolyte. The electrolyte is responsible for transferring electrons between

the two electrodes. The dye plays a crucial role in absorbing light, converting photons into excited electrons and transferring electrons to semiconductors [7, 8].

Dye is the most important component of DSSC whose performance in photoabsorption is directly related to cell efficiency. It can produce higher efficiency if covers a broad range of light spectrum [9]. However, the absorption spectrum of dyes substantially shows one or few peaks in the visible light spectrum [10]. Cosensitizing is one of the best methods for widening the photoabsorption spectrum of DSSCs. Most of the work done is based on a mixture of two or more different dyes, which is known as the Cocktail method [11–19]. However, the considerations such as dye…dye interaction [20], electron quenching [21], and dye partial loading [10] have been led to the development of other methods such as sequential sensitization [21–24], dye stacking [25], selective positioning [26–28], heterogeneous positioning [29, 30], dye mixture design [31, 32], ALD [33, 34], and ultrafast cosensitization [35]. Dyes used in DSSCs fall into two general categories: synthetic and natural. The synthetic dyes have shown higher efficiencies due to more efficient electron injection and the presence of suitable ligands to provide more tightly bind to the surface of titanium dioxide [8]. Various studies have been developed to investigate the DSSC cosensitization using different synthetic dyes with different peaks in their absorption spectra [11–14]. However, these dyes are expensive and have a complex manufacturing process. Indeed, the design and the use of several synthetic dyes with different peaks in the absorption spectrum dramatically increase the cost of solar cell construction [36]. In contrast, natural dyes extracted from plants are cheap and environmentally friendly. Also, these types of dyes have a straightforward manufacturing process with a broad variety [4]. Various studies have been developed to investigate the DSSC cosensitization using natural dyes [15–19], but these dyes usually do not bind very tightly to titanium dioxide nanoparticles causing a lower efficiency [7, 37].

The conventional cosensitization methods used only a few synthetic dyes or only a few natural dyes. Simultaneous use of synthetic dyes with natural dyes can take advantage of both, which has received less attention. Therefore, the aim of this study is to propose a new approach for spectral expansion of DSSC using both synthetic and natural dyes. In this case, while we can use the capabilities of synthetic dyes in strong bonding and electron injection to semiconductor, we can use inexpensive natural dyes to improve the synthetic dye spectrum and develop the cell absorption spectrum without the need for multiple-synthetic dye design. Most previous studies have focused on employing the cocktail method. Pratiwi et al. used a cosensitization method by adding N719 synthetic dye in the different volumes of anthocyanin natural dye [38]. ZU et al. investigated the impact of cosensitization of anthocyanin and chlorophyll with N719 on DSSC performance [39]. Richhariya and Kumar performed a cosensitization of DSSC using a mixture of Eosin-y with Hibiscus-sabdariffa [40]. Madili et al. investigated the combination of lawsone and D131 dyes for DSSC cosensitization [41]. A composition of chlorophyll and various ruthenium dyes was studied by Pratiwi et al. [42]. Msangi et al. investigated the combination of crocetin and D205 for DSSCs cosensitization [43]. All of these approaches were based on mixing the dyes. But this technique has several restrictions, which have been mentioned before. Kumar et al. used the sequential method [44], but this method can hurt dye loading [10]. Also, the natural dyes are neutralized if sensitization of the semiconductor layer with natural dyes is performed in the presence of synthetic dyes with a strong bond into the semiconductor [20]. In the present study, a new methodology for the cosensitization by natural and synthetic dyes is proposed using bilayer deposition of $TiO_2$ to increase the optical absorption of DSSCs. The bilayer or multiple-layer structure has had several applications in DSSCs. Most of them can be categorized as follows: (i) creating multiple layers to enhance the light scattering, increase the effective surface, and prevent the charge recombination (compact blocking layer deposition) [45, 46]; (ii) using bilayer or multiple layers of $TiO_2$ with different nanostructure or morphology to improve the light-harvesting or charge transportation [47, 48]; (iii) use of a layer consisting of a material with different optical and electrical properties from $TiO_2$ as $TiO_2$ complement [49–53]; (iv) producing a variation in the size of particles and porosity of layers [54]; (v) plasmonic enhancement of cell using a layer composed of metal nanoparticles [55, 56]; (vi) the usage of multilayer structure to optimize the thickness [57]; and (vii) charge transfer improvement by multilayer $TiO_2$ deposition using various precursors [58]. In all of the above methods, the monosensitization or cosensitization is performed for all layers similarly. According to our review, the only study that used bilayer $TiO_2$ for separate sensitization was recently presented by Fu et al. [59]. But both of the dyes used in this study were synthetic, which principally increases costs. Also, its press-based bilayer method creates double complexity in the manufacturing process. Our proposed approach is based on bilayer structure for separated sensitization at no extra cost. To compare the proposed method with conventional cosensitization methodology, the cosensitization was done in three ways. In the first method, similar to most previous works, the semiconductor layer was sensitized by a mixture of synthetic and natural dyes (cocktail method). The sequential method was used as the second method, in which the sensitization was performed for each dye in a separate step. A novel approach was proposed as the third method. To overcome the problems of other methods in simultaneous dye adsorption, the semiconductor deposition was performed in two steps. Each layer was sensitized separately by one type of dye. The bottom layer was deposited via the conventional method. However, a low-temperature methodology was used for the top layer deposition. The developed procedure for fabricating solar cells is presented in Section 2. Then, the results are discussed in Section 3. The extracted dyes were characterized by UV-visible and FT-IR spectroscopy to study the photoabsorption spectrum and anchoring groups of the dyes. Also, XRD, FESEM, and EDS analyses were performed to evaluate the semiconductor layers in terms of crystalline phase, morphology, elemental mapping, and porosity. Besides, the electrical performance of the

fabricated solar cells was examined by electrochemical impedance spectroscopy (EIS) and J-V characterization.

## 2. Experimental Study

*2.1. Materials.* Ethanol 99.9%, hydrochloric acid 37%, titanium tetra isopropoxide (Ti [OCH(CH3)2]4), and N719 synthetic dye (bis(2,2_-bipyridyl-4,4_-dicarboxylato)-ruthenium (II)) were purchased from Sigma Aldrich. DI-water, TiO2 paste. Pt paste, iodide/tri-iodide electrolyte, and FTO glasses (whit S-R < 8 $\Omega$cm$^{-2}$) were purchased from Sharif Solar Co.

*2.2. Dye Extraction.* To cover a wider range of photoabsorption spectra, N719 was used as a synthetic dye, and betanin, crocin, acacetin, and indigo were used as natural dyes, which are extracted from beetroot, saffron, Acacia-nilotica, and Indigofera, respectively. To extract betanin, a beetroot was washed, dried, and cut into small pieces. 50 g of them was put into a beaker containing 100 ml of ethanol and ultrasound at 45°C for 15 minutes and then was kept in a dark place at room temperature for 24 hours. For the other three dyes, 0.5 g of the powder from the dried leaves of each plant separately was added to 10 ml of ethanol and ultrasound at 45°C for 15 minutes and then kept in a dark place at room temperature for 24 hours. Then, the solutions were strained and stored at 4°C.

*2.3. Fabrication of DSSCs.* In this study, three types of DSSC were fabricated: mixed dye-sensitized solar cell (MDSSC), sequential dye-sensitized solar cell (SDSSC), and bilayer dye-sensitized solar cell (BLDSSC).

For all three types, the FTO glass has been used as electrode substrate. They were cut into $2 \times 1.5\,\text{cm}^2$ dimensions and washed three times with suds, deionized water, and ethanol.

To create the photoanode in MDSSC type, the titanium paste was coated on a piece of FTO glass and annealed at 450°C for half an hour. After cooling and reaching room temperature, it was immersed in a mixture of synthetic and natural dyes solution and kept for 24 hours. Three mixed dye solutions were made with different volume ratios. In this case, the solar cells sensitized by these solutions were called MDSSC1, MDSSC2, and MDSSC3.

In SDSSCs, a similar procedure was performed for $TiO_2$ deposition. However, the fabricated photoanodes were sequentially immersed in individual dye solutions and kept in each solution for 24 hours. The photoanodes were cleaned with DI-water and ethanol after each sequence of sensitization to remove the unabsorbed dyes. In this regard, two sensitization modes were examined. In the first mode, the natural and synthetic dyes were utilized for the first and second phases of sensitization, respectively. An adverse procedure was carried out in the second mode. These solar cells were called SDSSC1 and SDSSC2, respectively.

To create the photoanode in BLDSSC type, first, a layer of titanium paste was coated on a piece of FTO glass and annealed at 450°C. Then, they were immersed in the natural dye solution and kept for 24 hours. After removing photoanodes from the solution, they were washed and dried to be prepared for the second stage of titanium dioxide deposition. Generally, dyes are organic materials that are sensitive to heat, so for the second layer, a low-temperature process was utilized using the method presented by Cole et al. [60]. For this purpose, 8.1 ml of titanium tetra isopropoxide was poured over 80 ml deionized water. Then, hydrochloric acid was added dropwise and stirred for four hours at room temperature. Also, three acid concentrations were tested (0.25 M, 0.5 M, and 1 M). After coating the second layer, the photoanodes were placed in the furnace. In addition, two different annealing temperatures were tested, including 120 and 450°C. The sample annealed at 450°C was called HT. Also, the samples made by three acid concentrations were annealed at 120°C. Thus, the prepared samples with these acid concentrations were called LT1, LT2, and LT3, respectively. The prepared photoanode was then immersed in the synthetic dye solution and kept for 24 hours. The solar cells fabricated with these photoanodes were named BLDSSC1, BLDSSC2, BLDSSC3, and BLDSSC4. The sensitization methods and the synthesis conditions used for each type of fabricated solar cell are tabulated in Table 1.

Next, to create the counter electrodes, the Pt paste was coated on the FTO glasses and annealed at 450°C. Then, the two electrodes were sandwiched on top of each other, and the electrolyte was injected between them. To prevent electrolyte leakage, sealing was performed by Serlin polymer. It should be noted that each type of solar cell was fabricated three times according to the above methods (batch size = 3), which in the repetition of each method, close results were obtained. However, in this article, the best results of each method are reported.

## 3. Results and Discussion

*3.1. Dye Characterization.* In general, dyes play a principal role in the functionality of the DSSCs. Five dyes were used in this study. The first dye was N719, which is one of the most efficient synthetic dyes [61]. It is composed of ruthenium metal—a high electron donator—in combination with polypyridine and COOH ligands that can bind very tightly to titanium dioxide nanoparticles [5, 62]. The other dyes are natural dyes that were extracted in an inexpensive and environmentally friendly way from beetroot, saffron, Acacia-nilotica, and Indigofera. The chemical structure of the dye molecules is shown in Figure 1. Due to their carboxyl, carbonyl, imine, and hydroxyl groups, these dyes can be linked to the surface of $TiO_2$ nanoparticles in the form of monodentate chelation, bidentate chelation, and bidentate bridging [62–68].

*3.1.1. UV-Visible Study.* The natural dyes were selected to cover a broad range of light absorption spectra. UV-visible spectroscopy was performed using PG Instruments T80 spectrophotometer to study the optical absorption of these dyes. The obtained photoabsorption spectra are depicted in Figure 2. Betanin showed a peak at 526 nm which indicates the HOMO (highest occupied molecular orbital) to LUMO (lowest unoccupied molecular orbital) transition of

Table 1: The sensitization methods and the synthesis conditions of fabricated solar cells.

| Cell type and code | Cosensitization method | Special condition of each type | | |
|---|---|---|---|---|
| Type 1 | Cocktail | The ratio of synthetic dye to each of the natural dyes | | |
| MDSSC1 | | 4 : 1 | | |
| MDSSC2 | | 2 : 1 | | |
| MDSSC3 | | 1 : 1 | | |
| Type 2 | Sequential | Sensitization steps | | |
| SDSSC1 | | Step 1: natural dyes step 2: synthetic dye | | |
| SDSSC2 | | Step 1: synthetic dye step 2: natural dyes | | |
| Type 3 | Separated (bilayer) | Photoanode code | HCL concentration (M) | Annealing temperature (°C) |
| BLDSSC1 | | HT | 0.25 | 450 |
| BLDSSC2 | | LT1 | 1 | 120 |
| BLDSSC3 | | LT2 | 0.5 | 120 |
| BLDSSC4 | | LT3 | 0.25 | 120 |

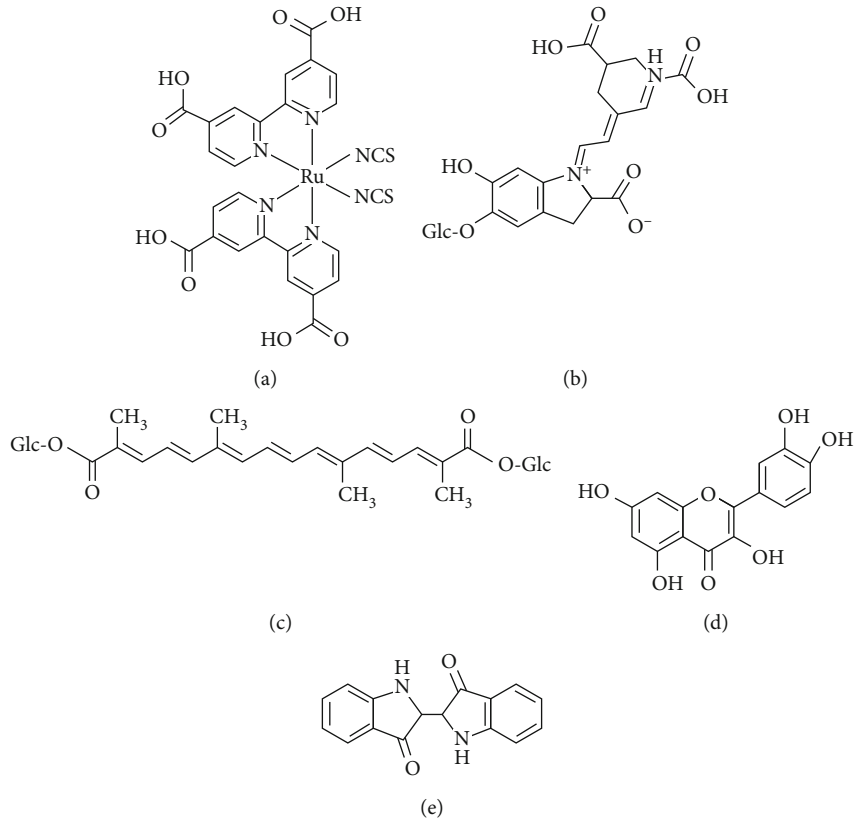


Figure 1: The chemical structure of (a) N719 [60], (b) betanin [18], (c) crocin [66], (d) acacetin [67], and (e) indigo [68].

nonbonding electrons located on the N-atoms via $\pi$-conjugated system [18]. Crocin indicated two peaks at 318 nm and 453 nm, which could be due to $n \longrightarrow \pi^*$ and $\pi \longrightarrow \pi^*$ transitions of electrons around the regions of C-H and C=C [65]. The spectrum of this dye showed good light absorption in the range of 400 to 470 nm [66]. Acacetin displayed a broad absorption spectrum, ranging from 300 to 400 nm with several consecutive peaks from 315 to 391 nm, which can be due to HOMO to LUMO transitions of electrons on O and C=C regions [67, 69]. Indigo shows two peaks at 410 nm and 665 nm that could be due to electron transitions from C=C and NH donor to C=O acceptor and indicates light absorption in the NIR region [18, 68]. As shown in Figure 2(e), a cosensitization with these dyes can produce a broad spectrum that covers most of the visible area.

*3.1.2. FT-IR Analysis.* To investigate the chemical structure and functional groups of dyes, FT-IR spectroscopy was performed using Thermo Nicolet AVATAR 370 Spectrometer. The results are shown in Figure 3. The peaks located at

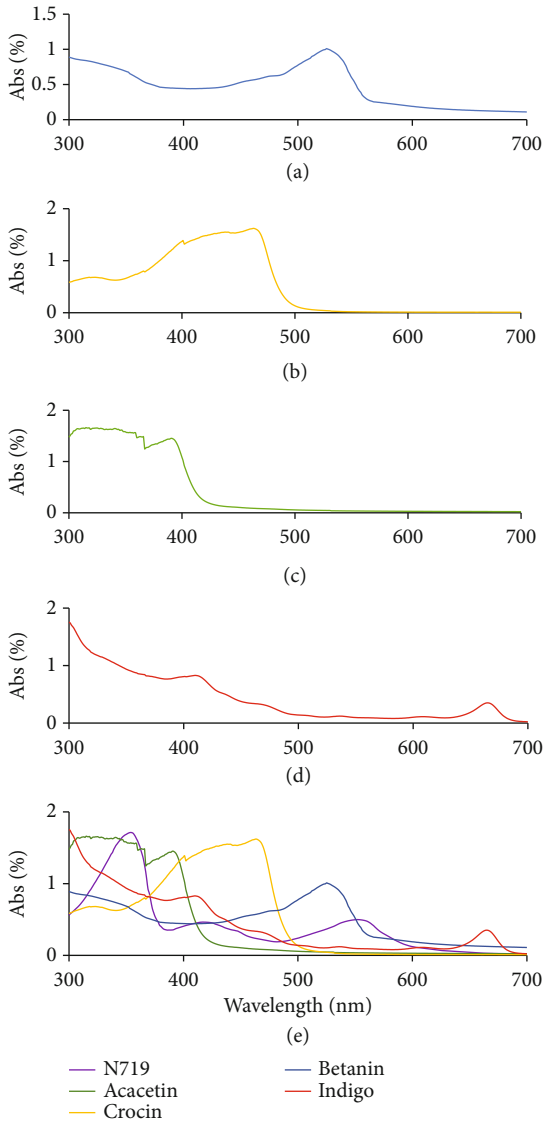


Figure 2: The UV-visible spectra of (a) betanin, (b) crocin, (c) acacetin, (d) indigo, and (e) the five dyes used.

3511 $cm^{-1}$, 3487 $cm^{-1}$, and 3366 $cm^{-1}$ in the IR spectra of indigo, betanin, and N719 can be assigned to N-H bond in the heterostructure and aromatic amines [70]. The stretching vibration of O-H bonds in the hydroxyl groups caused the peaks at 3402 $cm^{-1}$, 3410 $cm^{-1}$, 3423 $cm^{-1}$, and 3408 $cm^{-1}$ in the spectrums of betanin, crocin, acacetin, and indigo, respectively [71]. Besides, the peaks located at 2960 $cm^{-1}$, 2926 $cm^{-1}$, and 2857 $cm^{-1}$ in the spectra of betanin and crocin can be related to the stretching vibration of C-H bonds [72]. The peak located at 2091 $cm^{-1}$ in the spectrum of N719 can be assigned to isothiocyanate groups [73]. The peaks that appeared at 1721 $cm^{-1}$, 1745 $cm^{-1}$, and 1713 $cm^{-1}$ in the spectra of betanin and N719 correspond to COOH carboxylic groups [73]. Also, the peaks located at 1613 $cm^{-1}$, 1615 $cm^{-1}$, 1628 $cm^{-1}$, and 1632 $cm^{-1}$ in the spectrum of N719, betanin, crocin, and indigo can be assigned to the stretching vibration of C=C and C=O bonds or bending vibration of C-H bonds [73, 74]. The peak that appeared at 1517 $cm^{-1}$ in the spectrum of betanin corresponds to aromatic nitro compounds. Furthermore, the presence of $COO^-$ in the structure of this dye can cause an absorption peak at 1470 $cm^{-1}$ [73]. The peaks located at 1401 $cm^{-1}$ in the spectrums of Indigo can be assigned to the stretching vibration of C=N in the aromatic amine [75]. Also, the peak that appeared at 1462 $cm^{-1}$ in the spectrum of N719 can be assigned to the stretching vibration of C=C-C in the aromatic rings [73]. The peaks that appeared at 1059 $cm^{-1}$, 1065 $cm^{-1}$, and 1096 $cm^{-1}$ in the spectra of N719, indigo, and betanin are related to stretching vibration of C-N bonds [76]. The bending vibration of C-H bonds caused the peaks at 1385 $cm^{-1}$, 1384 $cm^{-1}$, and 997 $cm^{-1}$ in the spectrums of crocin and acacetin [73, 76]. Besides, the stretching vibration of C-O bonds caused the peaks at 1047 $cm^{-1}$ and 1051 $cm^{-1}$ in the spectrums of crocin and acacetin, respectively [76]. Furthermore, the peaks located at 615 $cm^{-1}$ and 604 $cm^{-1}$ in the spectrums of acacetin and indigo can be assigned to the out-of-plane vibration of O-H bonds [73].

*3.2. Characterization of TiO2 Layers.* As mentioned before, the top layer of photoanodes was created in four modes. The first was based on the high-temperature process (HT). The other modes were based on a low-temperature process with three acid concentrations (LT1, LT2, and LT3). The XRD, FESEM, and EDS analyses were employed to assess the properties of these layers.

*3.2.1. XRD Analysis.* The XRD analysis was performed using a Philips diffractometer with CuKa irradiation ($k = 1.5406$ A°) on HT, LT1, LT2, and LT3 samples. The results are shown in Figure 4. For the HT sample, the $2\theta$ peaks at 25.19, 37.39, 47.84, 51.9, 61.64, and 77.89 correspond to (1 0 1), (0 0 4), (2 0 0), (2 0 2), (2 1 3), and (2 0 6) crystal planes assigned to tetragonal structure of anatase $TiO_2$ (ICDD-ref: 96-900-8217). Also, the peaks observed at 35.86, 54.04, and 65.19 are related to the (1 0 1), (2 1 1), and (2 2 1) crystal planes, which correspond to the rutile phase (ICDD-ref: 96-900-414). For LT1, LT2, and LT3 samples, the peaks at 25.29, 37.69, 47.9, 51.9, and 78.44 correspond to the (1 0 1), (0 0 4), (2 0 0), (2 0 2), and (2 0 6) crystal planes assigned to anatase phase (ICDD-ref: 96-900-8215). Furthermore, the two peaks at 35.86 and 65.13 correspond to (1 0 1) and (2 2 1) planes assigned to the rutile phase (ICDD-ref: 96-900-4147). In addition, the LT3 sample showed another peak at 62.04, which is related to the (2 1 3) plane of the anatase phase. Besides, the LT1 sample showed another peak at 54.04 related to the (2 1 1) plane of the rutile phase. Also, the LT2 and LT3 samples showed two peaks at 30.84 and 55.28 corresponding to (1 2 1) and (1 4 2) planes assigned to the orthorhombic structure of the brookite phase (ICDD-ref: 96-900-4138).

According to the results, the acid concentration affected the formation of the anatase, rutile, and brookite phases [77]. In this case, the anatase phase was purer at lower acid concentration, but the purity of the anatase phase decreased at higher acid concentration, and the amount of rutile phase formation increased. This can be due to the amount of $OH^-$ ligands [78]. The probability of $TiO_6^{2-}$ octahedra edge-

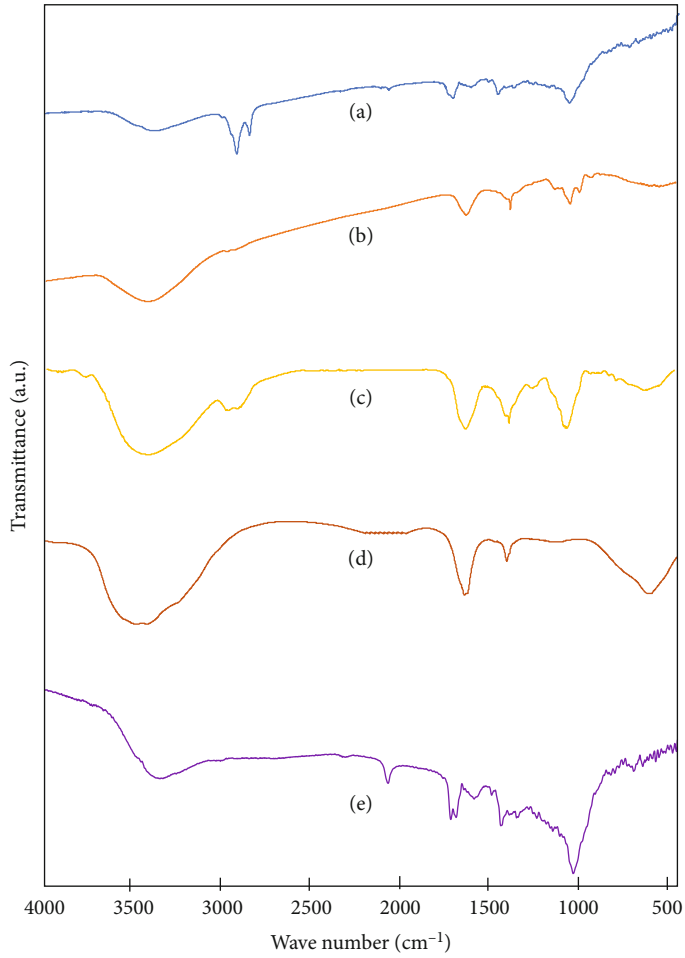


Figure 3: The FT-IR spectra of (a) betanin, (b) crocin, (c) acacetin, (d) indigo, and (e) N719.

sharing increases at lower acid concentrations with more $OH^-$ ligands. This situation leads to the formation of the anatase phase. In contrast, at lower acid concentrations with fewer $OH^-$ ligands, the probability of edge-sharing that needs two simultaneous dehydration reactions decreases, and the probability of corner-sharing increases. These situations cause the formation of the rutile phase. A decline in the acid concentration leads to the emergence of the brookite phase. In this regard, the highest amount of brookite phase occurred in the intermediate state (LT2), which indicates the simultaneous creation of edge and corner-sharing and the change from rutile to anatase structure with decreasing acid concentration [78–82]. In addition, Gaynor et al. [83] reported that an increase in the acid concentration had a considerable effect on the aggregation of $TiO_2$ cores and the formation of larger particles. The size of the nanocrystals can be obtained using the Debye-Scherer relationship [84]:

$$D = \frac{0.9\lambda}{\beta \cos\theta}, \quad (1)$$

which $\lambda$ is the wavelength of the radiated beam, $\theta$ is the Bragg diffraction angle, and $\beta$ is the full width at half maximum of the strongest peak (FWHM). The calculated values for the samples are given in Table 2.

*3.2.2. FESEM.* Figure 5 displays the FESEM images of the HT, LT1, LT2, and LT3 samples taken from the Mira3-TEscan with HV:15KV in three resolutions. Also, the elemental mapping of these layers via EDS analysis is shown in Figure 6 indicating the synthesis of $TiO_2$ NPs.

In the FESEM image of the HT sample, a completely porous morphology with uniform and relatively spherical grains was observed. The particles were joined together, and almost no agglomeration was observed. The grain size distribution histogram measured for 100 particles is shown in Figure 7(a). The average grain size of this sample was 26.9 nm with a standard deviation of 5.7. The LT1 sample has been lumped. However, the FESEM image of the LT2 and LT3 samples illustrate that decreasing the acid concentration resulted in a more uniform morphology, higher crystallinity, and better porosity at an annealing temperature of 120°C. In this case, the LT3 sample is fully comparable to the HT sample and showed the least agglomeration between low-temperature modes. The size distribution histogram of the LT2 and LT3 samples are shown in Figures 7(b) and 7(c), respectively. Their average grain sizes were 31.2 and 24.7, with a standard deviation of 7.07 and 6.2, respectively.

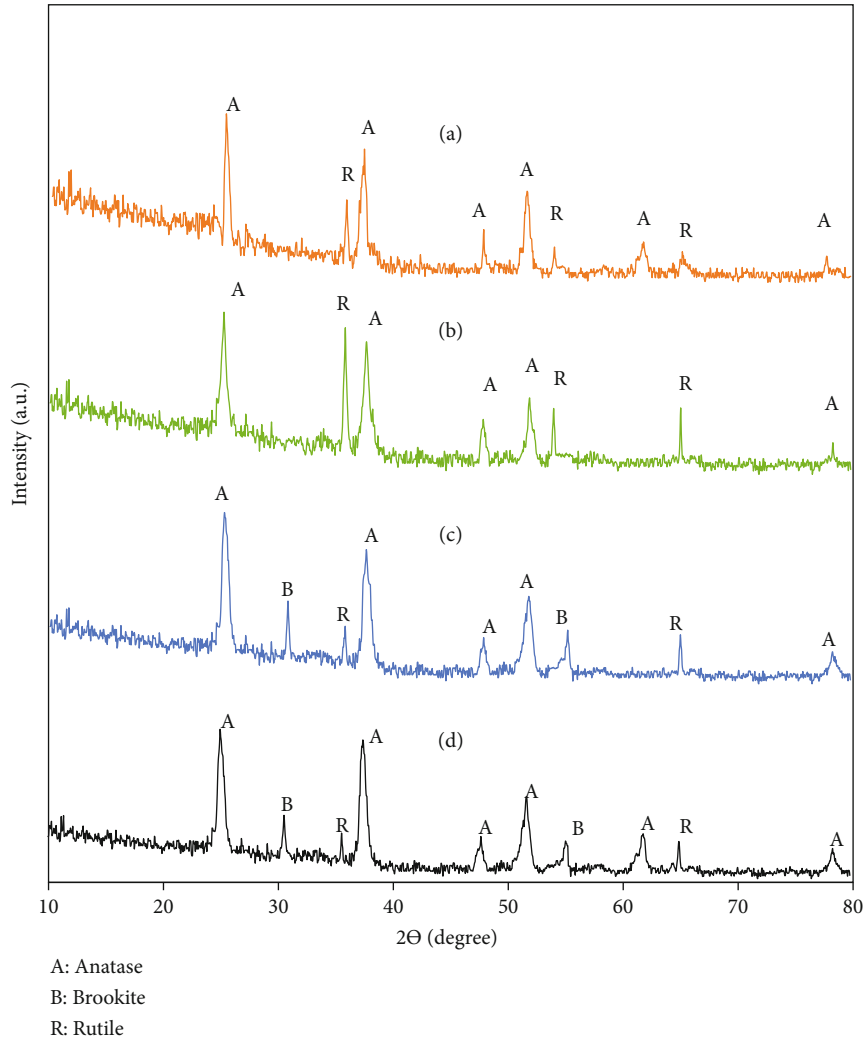


Figure 4: The XRD spectrum of (a) HT, (b) LT1, (c) LT2, and (d) LT3.

Table 2: Calculated values for crystallinity state and nanocrystal size of layers.

| Layer | $\lambda$ (Å) | $2\theta$ (degree) | FWHM | Crystallinity degree (%) | Estimated crystalline phase composition percentages (%) | D (nm) |
|---|---|---|---|---|---|---|
| HT | 1.5406 | 25.19 | 0.393 | 64.21 | A: 68.34 R: 32.66 | 20.6 |
| LT1 | 1.5406 | 25.29 | 0.295 | 47.19 | A: 54.82 R: 45.18 | 27.3 |
| LT2 | 1.5406 | 25.29 | 0.344 | 55.43 | A: 61.21 R: 20.26 B: 18.53 | 22.8 |
| LT3 | 1.5406 | 25.29 | 0.445 | 58.75 | A: 64.36 R: 17.75 B: 17.79 | 18.3 |

A: anatase; R: rutile; B: brookite.

*3.3. Electrical Properties of DSSCs.* The electrical performance of fabricated solar cells was evaluated by the EIS and J-V characteristics to investigate their charge transfer process and photovoltaic performance.

*3.3.1. Electrochemical Impedance Spectroscopy.* To assess the charge transfer process, EIS analysis was performed using GWInstek-8000G LC-Meter. The achieved Nyquist diagrams are shown in Figure 8. The diagrams consist of two semicircles, which the left semicircle with a diameter of $R_1$ is related to charge transfer at the counter electrode and the redox process between Pt and the electrolyte, and the right semicircle with a diameter of $R_2$ is related to charge-transfer resistance at the TiO2/dye/electrolyte interface. The intersection point of the curves with the horizontal axis indicates the constant series resistance ($R_0$), which is mainly related to the sheet resistance of FTO and the charge diffusion within the semiconductor layer [85, 86].

As shown in Table 3, the amount of $R_1$ resistances for all types of solar cells were close to each other because there was no difference between them in terms of counter electrodes. As is clear, the surface structure of the semiconductor layer

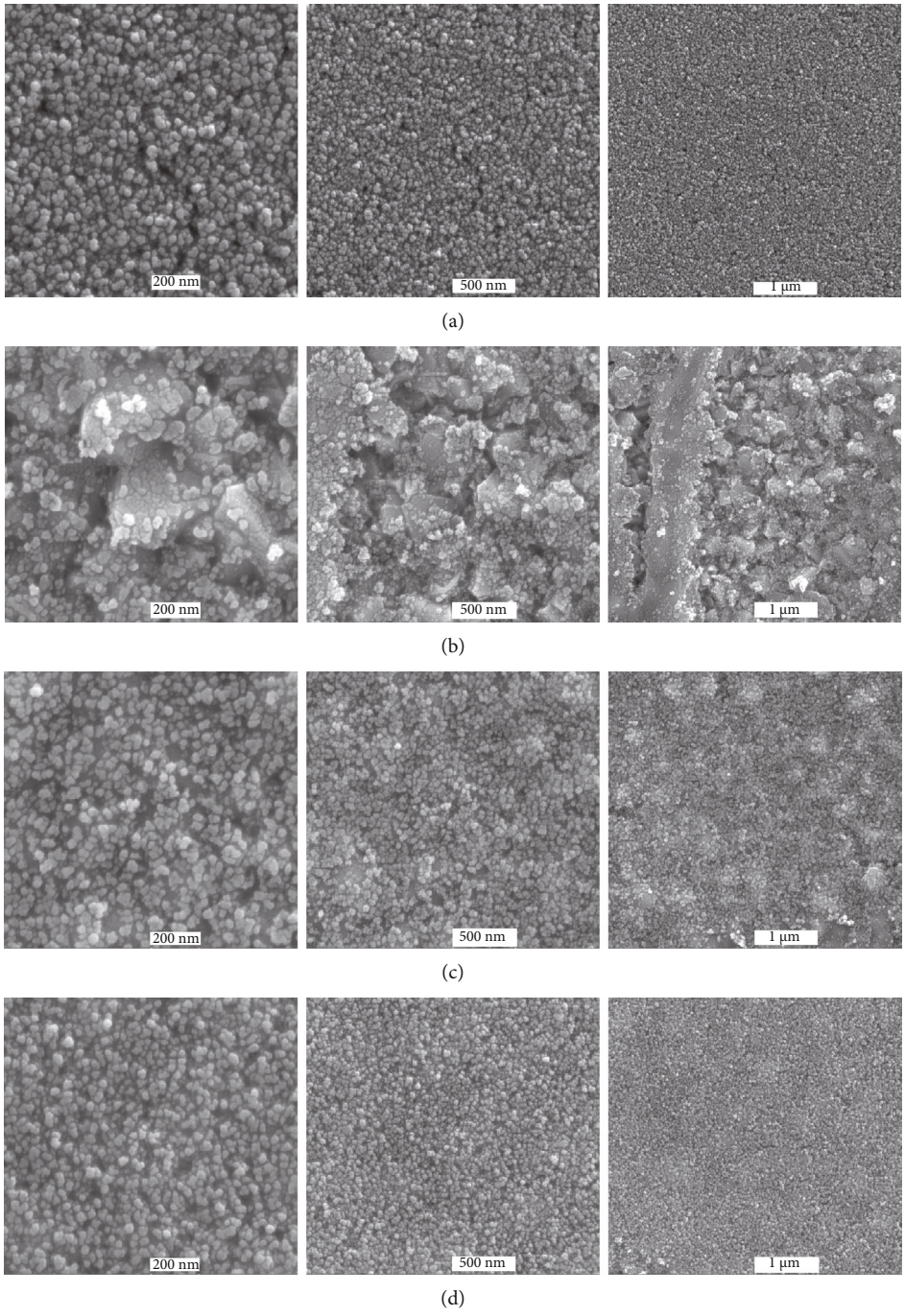


Figure 5: The FESEM image of (a) HT, (b) LT1, (c) LT2, and (d) LT3, in three resolutions.

completely affected the resistance of $R_2$. The BLDSSC2 and BLDSSC3 cases, which have lower crystallinity and less morphology uniformity, have shown more resistance. The presence of residual radicals on the surface of nanoparticles creates the electronic states, which are known as surface states [87]. This situation provides a recombination process in addition to the recombination process of the electrons at the conduction band of $TiO_2$ [88]. Also, improving the crystallinity, in addition to reducing the surface states, reduces the bulk traps caused by the amorphous regions between the crystals [87]. It has also been shown that the rutile phase produces higher resistance compared to anatase [89, 90]. For this reason, the BLDSSC4 and BLDSSC1 modes of the third type of fabricated solar cells, which like the first and second types (SDSSC and MDSSC) had a high-quality semiconductor layer and anatase phase purity, have shown less resistance. Also, the diversity of dyes adsorbed to the semiconductor affects this resistance because the injected electrons cause more fermi level shifting [10]. In this regard, the BLDSSC4 and SDSSC samples, which are separately sensitized by natural and synthetic dyes, have shown less resistance than MDSSCs.

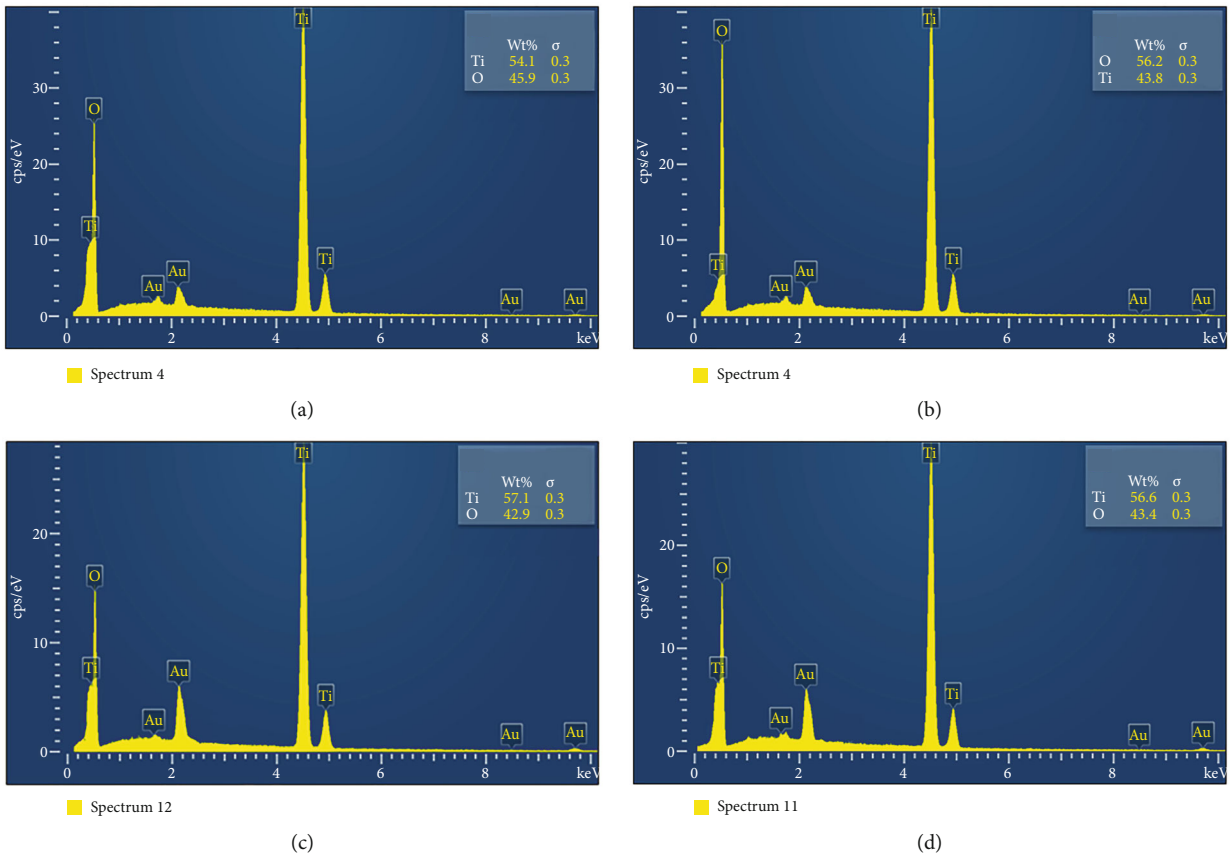


Figure 6: The EDS profile of (a) HT, (b) LT1, (c) LT2, and (d) LT3.

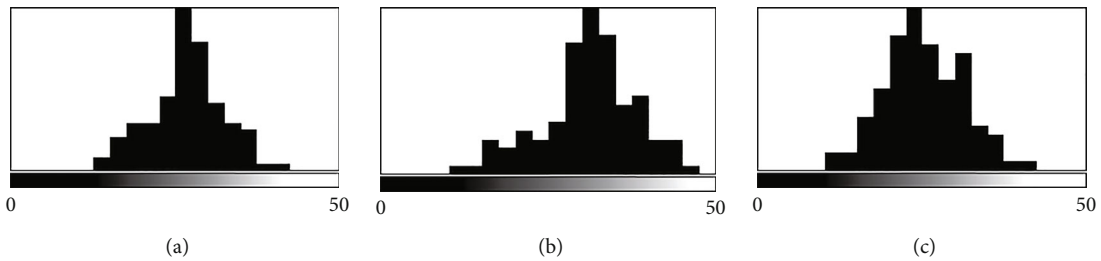


Figure 7: The size distribution of layers: (a) HT, (b) LT2, and (c) LT3.

All modes of the first two types of fabricated solar cells had approximately the same resistance values of $R_0$. These resistance values were less than all four modes in the third type of solar cell. Also, the sheet resistance value of FTO was the same in all cases. But the charge diffusion inside the semiconductor layer of the third type of fabricated solar cells is more resistant than other types. This situation can be due to more grain boundaries resulting from two-stage deposition. It has been shown that the presence of more bulk traps causes more resistance to charge transportation inside the semiconductor [70]. For this reason, in the third type of solar cells, the highest value of $R_0$ was achieved for BLDSSC2, while the lowest value was achieved for BLDSSC1. Although the semiconductor layer in BLDSSC3 had lower crystallinity than BLDSSC4, its larger particle size can cause fewer grain boundaries.

*3.3.2. Photovoltaic Properties.* The photovoltaic performance of fabricated solar cells was investigated by measuring their J-V characteristics under 100 mW/cm$^2$ white light radiations with an AM1.5 filter using the Irasol284 solar simulator system. The values obtained for open-circuit voltage ($V_{oc}$), short-circuit current density ($J_{sc}$), fill factor (FF), and efficiency are listed in Table 4 compared to other studies that have used different cosensitization methods.

The first type of solar cell was sensitized by a mixture of natural and synthetic dyes with different volume ratios. The volume ratio of synthetic dye to each of the natural dyes was 4 : 1, 2 : 1, and 1 : 1 for MDSSC1, MDSSC2, and MDSSC3, respectively. As mentioned before, a batch consisting of three samples of each cell was made. The distribution of $J_{sc}$ and $V_{oc}$ of the batches are depicted in Figure 9(a), where the diameter of bubbles showed the efficiencies. As is clear, the values

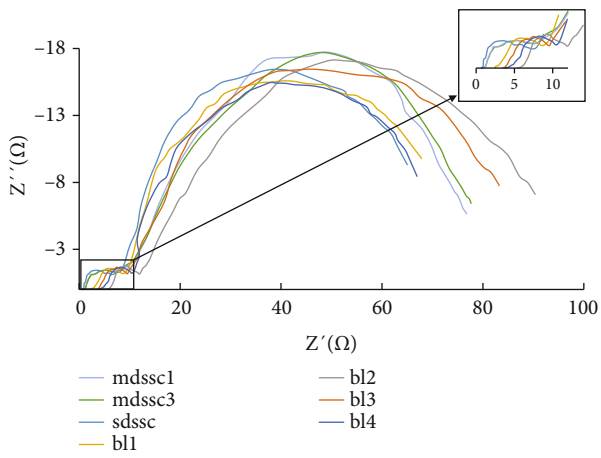


Figure 8: The achieved Nyquist diagrams from EIS analysis of fabricated solar cells.

Table 3: The resistances of fabricated solar cells achieved from EIS analysis.

| Solar cell name | $R_0$ (Ω) | $R_1$ (Ω) | $R_2$ (Ω) |
|---|---|---|---|
| MDSSC1 | 0.75 | 6.23 | 59.47 |
| MDSSC2 | 0.69 | 6.25 | 59.85 |
| MDSSC3 | 0.81 | 6.19 | 61.12 |
| SDSSC1 | 0.67 | 5.85 | 50.15 |
| SDSSC2 | 0.72 | 5.91 | 48.76 |
| BLDSSC1 | 2.43 | 5.71 | 52.67 |
| BLDSSC2 | 5.34 | 5.62 | 71.15 |
| BLDSSC3 | 3.44 | 5.86 | 65.48 |
| BLDSSC4 | 3.76 | 6.14 | 49.82 |

obtained for the samples in each batch are very close. The MDSSC1 batch showed a median efficiency of 1.84% with a standard deviation of 0.035. The MDSSC2 batch showed a median efficiency of 1.82% with a standard deviation of 0.026. The MDSSC3 batch showed a median efficiency of 1.67% with a standard deviation of 0.02. Also, the values obtained for the MDSSC1 batch and MDSSC2 batch are very close. The best achieved efficiencies of the batches were 1.88% ($J_{sc} = 7.48\,mA/cm^2$, $V_{oc} = 437\,mV$, FF = 0.57), 1.85% ($J_{sc} = 7.52\,mA/cm^2$, $V_{oc} = 425\,mV$, FF = 0.58), and 1.69% ($J_{sc} = 8.22\,mA/cm^2$, $V_{oc} = 397\,mV$, FF = 0.52), respectively. It was found that the third model had lower efficiency than others. Also, the first two models provided a higher efficiency, but their characteristics were very close together. Therefore, it can be concluded that more volume of synthetic dyes than natural dyes could improve the efficiency, but more increments in the volume of synthetic dyes did not cause a greater effect. The *J-V* characteristics of the best results obtained for these solar cell models are displayed in Figure 9(b). Also, they were compared to a solar cell that was only sensitized by N719. All three MDSSC modes showed higher short-circuit currents than N719-sensitized solar cell. The MDSSC1 and MDSSC2 were not significantly different, but MDSSC3 showed more short-circuit current. Thus, in the cosensitization by mixed natural and synthetic dyes, natural dye performance may be impaired in the presence of a larger volume of synthetic dyes. This issue indicates a higher possibility of synthetic dye adsorption due to the carboxylic ligands with stronger binding to $TiO_2$ [96]. The $V_{oc}$ of solar cells was decreased from MDSSC1 to MDSSC3. The $V_{oc}$ of all three models is lower than the N719-sensitized solar cell. This issue could be due to energy levels resulting from the combination of dye molecules and the possibility of more electron recombination [20].

The second type of solar cells was sensitized separately by natural and synthetic dyes in two modes: in SDSSC1, the semiconductor layer was immersed first in the synthetic dyes and then in the natural dyes. But an adverse procedure has been carried out in SDSSC2. The distribution of $J_{sc}$ and $V_{oc}$ of each batch is displayed in Figure 10(a). The SDSSC1 batch showed a median efficiency of 2.15% with a standard deviation of 0.025. The SDSSC2 batch showed a median efficiency of 2.25% with a standard deviation of 0.03. The best obtained efficiencies of the batches were 2.19% ($J_{sc} = 7.75\,mA/cm^2$, $V_{oc} = 492\,mV$, FF = 0.57) and 2.29% ($J_{sc} = 8.54\,mA/cm^2$, $V_{oc} = 488\,mV$, FF = 0.55), respectively. The *J-V* characteristics of the best results obtained for these solar cell models are displayed in Figure 10(b). This sensitization method showed higher efficiency than simultaneous sensitization. It can be concluded that because washing was done after each step of immersion, the aggregated dyes that do not bond to $TiO_2$ were cleaned, and the possibility of other dyes adsorption increased. Thus, the diversity of adsorbed dyes occurred more effectively. All samples of the SDSSC2 batch showed higher short circuit current and efficiency than the SDSSC1 batch. Therefore, it can be concluded that the dye absorption variety occurs more effectively if the sensitization is first performed by the natural dyes in comparison with the cases where the sensitization is performed first by synthetic dye or simultaneously. However, the diversity of SDSSC2 is slightly greater than that of SDSSC1, which could indicate greater sensitivity of natural dye adsorption to environmental conditions.

It was observed that at the cosensitization by both natural and synthetic dyes, the presence of each type of dye as well as their order and volume ratio can affect the absorption of other dye and consequently the overall performance of the solar cell. For this reason, in this study, a new method for cosensitization by natural and synthetic dyes has been proposed, in which the adsorption of natural and synthetic dyes is done by separate semiconductor layers. In this way, each type of dye has its independent effect on the performance of the solar cell without impressing by the other. For this purpose, in the third type of fabricated solar cells, the semiconductor was deposited in two layers. The bottom layer was sensitized by natural dyes, and the upper layer was sensitized by the synthetic dye. The conventional method of producing titanium dioxide nanoparticles requires annealing at temperatures above 450°C [97]. For the first mode of the third type of solar cell (BLDSSC1), both layers of semiconductor were created using this method, but no acceptable result was observed. The reason is that the natural dyes were practically damaged during the annealing process of the upper

Table 4: $V_{oc}$, $J_{sc}$, FF, and efficiency of fabricated solar cells.

| Method (name) | | Dye type | $V_{oc}$ (mV) | $J_{sc}$ (mA) | FF | $\eta$ | Reference |
|---|---|---|---|---|---|---|---|
| Cocktail | | Natural + natural | 270 | 1.16 | 0.34 | 0.11 | [91] |
| Cocktail | | Natural + natural | 473 | 1.12 | 0.68 | 0.36 | [19] |
| Sequential | | Natural + natural | 460 | 2.64 | 0.63 | 0.81 | [92] |
| Cocktail | | Synthetic + synthetic | 670 | 14.29 | 0.68 | 6.42 | [59] |
| Cocktail | | Synthetic + synthetic | 770 | 11.2 | 0.66 | 5.71 | [93] |
| Cocktail | | Synthetic + synthetic Organic | 730 | 8.4 | 0.5 | 5.6 | [94] |
| Separated (bilayer) | | Synthetic + synthetic | 700 | 15.5 | 0.68 | 7.45 | [59] |
| Cocktail | | Natural + synthetic | 380 | 3.1 | 0.35 | 0.41 | [42] |
| Cocktail | | Natural + synthetic | 430 | 2.49 | 0.51 | 0.54 | [38] |
| Cocktail | | Natural + synthetic organic | 670 | 4.01 | 0.6 | 2.02 | [40] |
| Cocktail | | Natural + synthetic organic | 640 | 4.66 | .7 | 2.09 | [48] |
| Cocktail | | Natural + synthetic organic | 300 | 2.84 | 0.35 | 0.3 | [95] |
| Sequential | | Natural + synthetic organic | 215 | .10 | .25 | .13 | [44] |
| Monodye | N719-SSC | Synthetic | 454 | 7.12 | 0.51 | 1.68 | Present study |
| | MDSSC1 | | 437 | 7.48 | 0.57 | 1.88 | Present study |
| Cocktail | MDSSC2 | | 425 | 7.52 | 0.58 | 1.85 | Present study |
| | MDSSC3 | | 397 | 8.22 | 0.52 | 1.69 | Present study |
| Sequential | SDSSC1 | | 492 | 7.75 | 0.57 | 2.19 | Present study |
| | SDSSC2 | Natural + synthetic | 488 | 8.54 | 0.55 | 2.29 | Present study |
| | BLDSSC1 | | 446 | 7.32 | 0.52 | 1.72 | Present study |
| Separated (bilayer) | BLDSSC2 | | 416 | 6.13 | 0.53 | 1.36 | Present study |
| | BLDSSC3 | | 531 | 9.76 | 0.55 | 3.05 | Present study |
| | BLDSSC4 | | 525 | 10.27 | 0.64 | 3.48 | Present study |

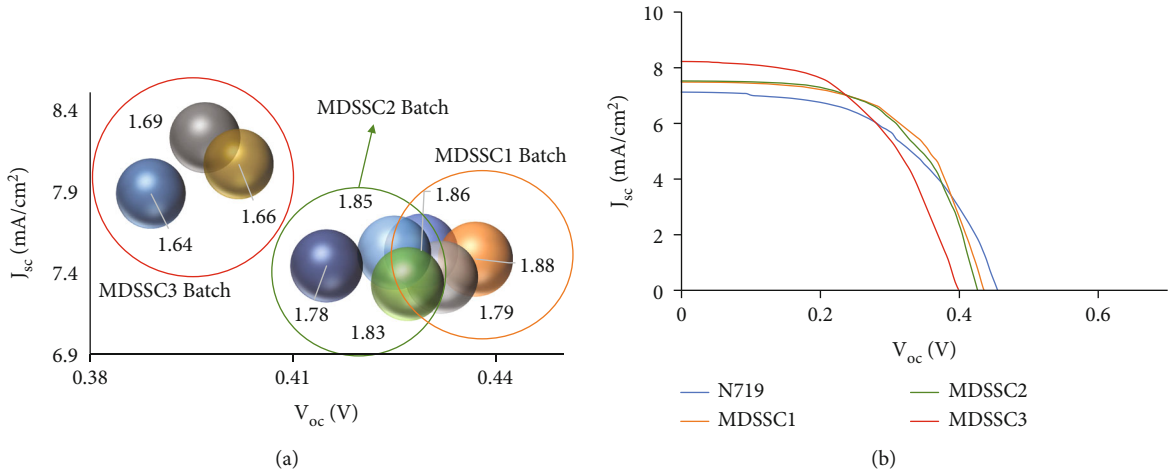


Figure 9: (a) The distribution of $J_{sc}$ and $V_{oc}$ of the MDSSC batches (the diameter of bubbles showed the efficiencies); (b) the $J$-$V$ characteristics of the best solar cell of each batch.

layer and loosed their function. A batch of this model consisting of three samples was fabricated. The distribution of $J_{sc}$ and $V_{oc}$ of the samples are shown in Figure 11(a). The median efficiency of this batch was 1.68% with a standard deviation of 0.016. The highest efficiency obtained for this mode was 1.72% ($J_{sc} = 7.32\,\text{mA/cm}^2$, $V_{oc} = 446\,\text{mV}$, FF = 0.52), which is not much different from the N719-sensitized cell. This outcome indicates that the natural dyes became completely ineffective. To solve this problem, a low-temperature process was used to create the upper layer. Since the crystalline structure, nanoparticle sintering, and layer morphology are completely dependent on the acid concentration [79], different acid concentrations were investigated for the other three modes (BLDSSC2, BLDSSC,3 and

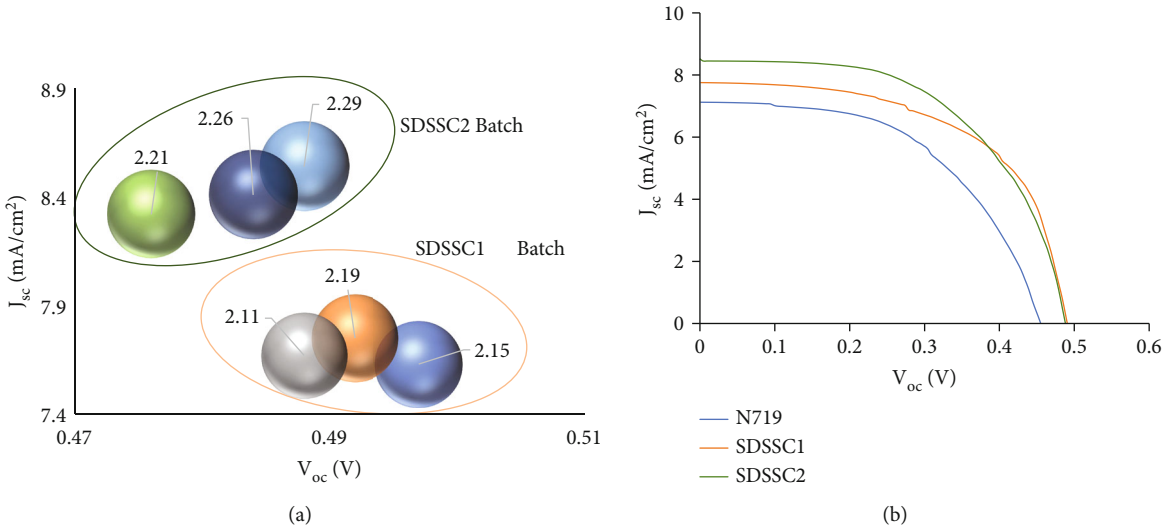


FIGURE 10: (a) The distribution of $J_{sc}$ and $V_{oc}$ of the SDSSC batches (the diameter of bubbles showed the efficiencies); (b) the $J$-$V$ characteristics of the best solar cell of each batch.

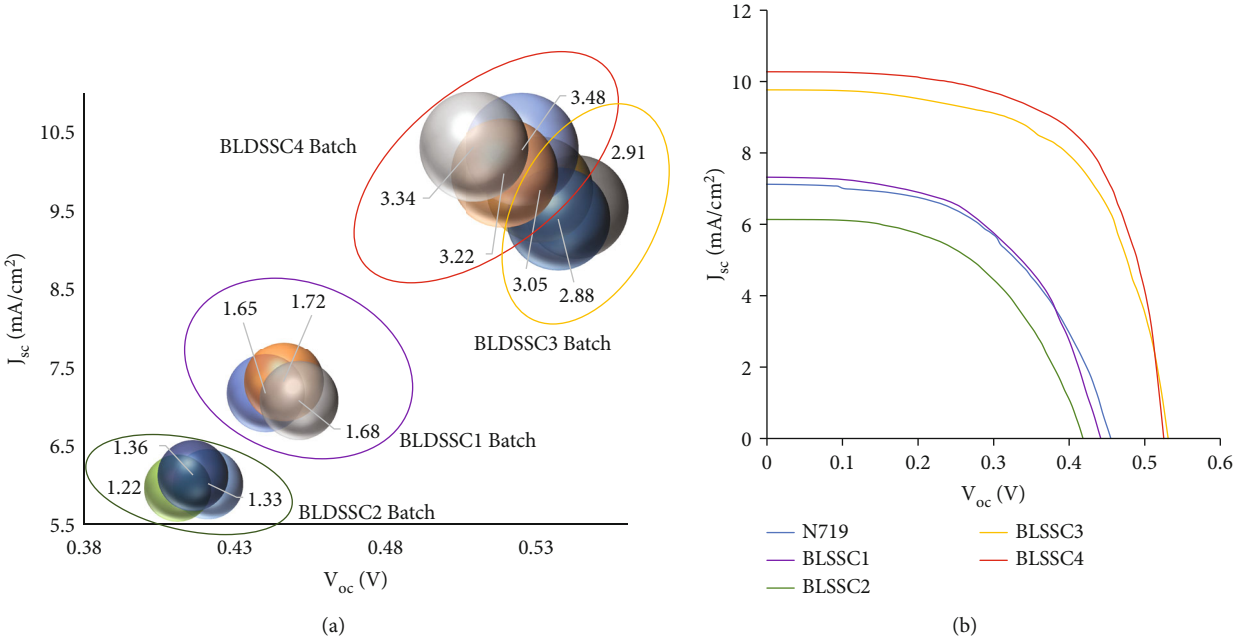


FIGURE 11: (a) The distribution of $J_{sc}$ and $V_{oc}$ of the BLDSSC batches (the diameter of bubbles showed the efficiencies); (b) the $J$-$V$ characteristics of the best solar cell of each batch.

BLDSSC4). The distribution of $J_{sc}$ and $V_{oc}$ of each batch is depicted in Figure 11(a). The median efficiency of the BLDSSC2 batch was 1.3%, and the highest efficiency achieved for this mode was 1.36% ($J_{sc} = 6.13$ mA/cm$^2$, $V_{oc} = 416$ mV, FF = 0.53). The BLDSSC2 provided the lowest performance among all fabricated solar cells due to the low crystallinity of its upper layer (LT1). In contrast, the BLDSSC3 and BLDSSC4 samples, which have a better crystalline structure and morphology, showed higher efficiencies. The median efficiency of these two batches was 2.94% and 3.34%, respectively, with standard deviations of 0.066 and 0.086. The highest efficiencies obtained for them were 3.05% ($J_{sc} = 9.76$ mA/cm$^2$, $V_{oc} = 531$ mV, FF = 0.55) and 3.48% ($J_{sc} = 10.27$ mA/cm$^2$, $V_{oc} = 525$ mV, FF = 0.64), respectively. The $J$-$V$ characteristics of the best results obtained for these solar cell models are shown in Figure 11(b). The open-circuit voltages of these two models were almost close together, but the highest values of the short-circuit current and the efficiency were achieved in the BLDSSC4. This situation occurred due to several reasons. The first reason was the adsorption increment of dyes because of the higher effective surface of the semiconductor structure. This higher effective surface was related to the spherical morphology, more suitable porosity [90], and

better electrolyte penetration inside the layer [89]. The second reason was dealt with its lower impedance due to the fewer surface states and bulk traps.

As it was observed, the conventional method of cosensitization by a mixture of natural and synthetic dyes cannot strongly improve the efficiency of the solar cell because dye…dye interaction caused more resistance toward the injection of electrons from the dye into the $TiO_2$ nanoparticles. Furthermore, it has been shown that the $V_{oc}$ of the solar cell is related to the density of electrons in the conduction band [98, 99], so the possibility of electron recombination in these traps can reduce the voltage and fill factor [100]. Also, the ineffectiveness of natural dyes prevents absorption spectrum expansion and light-harvesting. Thus, the current increment becomes negligible [10]. Therefore, the efficiency of this method was not more than the mono-dye sensitization method. Although the sequential sensitization method can resolve some limitations of the first method, producing a proper diversity of dyes still remains a major problem in this area. This problem takes place due to the limited capacity of $TiO_2$ sensitization, arising from the limited number of anchoring sites [20]. The use of the bilayer method for cosensitization by natural and synthetic dyes can cause separated adsorption of each type of dyes. Therefore, each dye had its independent effect on the spectral expanding of the solar cell as well as electron injection into the conduction band of $TiO_2$ nanoparticles [101]. In this regard, the proposed methodology provided two significant features at the same time: (i) the strong interaction between the $TiO_2$ nanoparticles and the donor atoms of synthetic dye molecules and (ii) the expansion of the light absorption spectrum using natural dyes. In addition, the enhancement in the variety of adsorbed dyes increased the density of injected electrons into the semiconductor. In this situation, the layer traps can be filled by some electrons leading to smoother transport of subsequent electrons [102]. Of course, to take advantage of these benefits, the fabricated layers in terms of crystallinity, porosity, and morphology must be of good quality, which completely affects the impedance of the solar cell and the process of charge injection and transportation [90, 103].

## 4. Conclusions

In this paper, a new approach for cosensitization of DSSC by synthetic and natural dyes was presented. This approach proposed a simple and low-cost methodology for enhancing the performance of DSSCs that may help the commercialization process. In this regard, four natural dyes were extracted inexpensively from plants to use as cosensitizers along with N719 synthetic dye to produce a broad photoabsorption spectrum. The proposed approach was compared to conventional cosensitization methods. The results indicated that the conventional cocktail method did not show a significant improvement compared to monodye sensitization due to limited adsorption of natural dyes in the presence of synthetic dyes with strong binding to $TiO_2$ nanoparticles. Also, the sequential method suffers from the limitation of subsequent dye adsorption due to limited $TiO_2$ anchoring sites. Therefore, in the present study, a bilayer structure with separate sensitization was proposed that each dye could have its independent effect on the photoabsorption and electron injection into the semiconductor. To prevent dye degradation within the annealing process of the top layer, a low-temperature process was performed for the top layer. The XRD and FESEM analyses showed that the layer created with an acid concentration of 0.25 M via the low-temperature process had good quality in terms of morphology, crystallinity, and porosity. The highest efficiency achieved in this method was 3.48%, which indicates the best performance of the proposed method in comparison with the cocktail and sequential methods that showed efficiencies of 1.88% and 2.29%, respectively. As the future direction, the photoabsorption enhancement of DSSCs can be studied using cosensitization by natural and inexpensive organic dyes based on the proposed approach to further reduce costs. Also, large-scale layering techniques such as roll-to-roll and printed-based processes can be developed for separated cosensitization.

## Data Availability

All data used to support the findings of this study are included within the article.

## Conflicts of Interest

The authors declare that they have no conflicts of interest.

## References

[1] A. Demirbaş, "Global renewable energy resources," *Energy Sources*, vol. 28, no. 8, pp. 779–792, 2006.

[2] M. A. Al-Alwani, A. B. Mohamad, N. A. Ludin, A. A. H. Kadhum, K. J. R. Sopian, and S. E. Reviews, "Dye-sensitised solar cells: development, structure, operation principles, electron kinetics, characterisation, synthesis materials and natural photosensitisers," *Renewable and Sustainable Energy Reviews*, vol. 65, pp. 183–213, 2016.

[3] J. Gong, K. Sumathy, Q. Qiao, Z. J. R. Zhou, and S. E. Reviews, "Review on dye-sensitized solar cells (DSSCs): advanced techniques and research trends," *Renewable Sustainable Energy Reviews*, vol. 68, pp. 234–246, 2017.

[4] N. Siregar, J. H. Panggabean, M. Sirait, J. Rajagukguk, N. S. Gultom, and F. K. Sabir, "Fabrication of dye-sensitized solar cells (DSSC) using Mg-doped ZnO as photoanode and extract of rose myrtle (*Rhodomyrtus tomentosa*) as natural dye," *International Journal of Photoenergy*, vol. 2021, Article ID 4033692, 7 pages, 2021.

[5] B. O'regan and M. Grätzel, "A low-cost, high-efficiency solar cell based on dye-sensitized colloidal $TiO_2$ films," *Nature*, vol. 353, no. 6346, pp. 737–740, 1991.

[6] U. Banin, N. Waiskopf, L. Hammarström et al., "Nanotechnology for catalysis and solar energy conversion," *Nanotechnology*, vol. 32, no. 4, article 042003, 2020.

[7] A. Bartolotta and G. Calogero, "Dye-sensitized solar cells: from synthetic dyes to natural pigments," in *Solar Cells and Light Management*, pp. 107–161, Elsevier, 2020.

[8] J. M. Juma, S. A. H. Vuai, and N. S. Babu, "TD-DFT investigations on optoelectronic properties of fluorescein dye derivatives in dye-sensitized solar cells (DSSCs)," *International*

*Journal of Photoenergy*, vol. 2019, Article ID 4616198, 8 pages, 2019.

[9] N. Zhou, K. Prabakaran, B. Lee et al., "Metal-free tetrathienoacene sensitizers for high-performance dye-sensitized solar cells," *Journal of the American Chemical Society*, vol. 137, no. 13, pp. 4414–4423, 2015.

[10] J. H. Yum, S. J. Moon, R. Humphry-Baker et al., "Effect of coadsorbent on the photovoltaic performance of squaraine sensitized nanocrystalline solar cells," *Nanotechnology*, vol. 19, no. 42, article 424005, 2008.

[11] M. Singh, R. Kurchania, R. Ball, and G. Sharma, "Efficiency enhancement in dye sensitized solar cells through step wise cosensitization of TiO 2 electrode with N719 and metal free dye," *IJPAP*, vol. 54, no. 10, 2016.

[12] Y. Zhao, F. Lu, J. Zhang, Y. Dong, B. Zhang, and Y. Feng, "Stepwise co-sensitization of two metal-based sensitizers: probing their competitive adsorption for improving the photovoltaic performance of dye-sensitized solar cells," *RSC Advances*, vol. 7, no. 17, pp. 10494–10502, 2017.

[13] A. Islam, T. H. Chowdhury, C. Qin et al., "Panchromatic absorption of dye sensitized solar cells by co-sensitization of triple organic dyes," *Sustainable Energy & Fuels*, vol. 2, no. 1, pp. 209–214, 2018.

[14] X. Wang, A. Bolag, W. Yun et al., "Enhanced performance of dye-sensitized solar cells based on a dual anchored diphenylpyranylidene dye and N719 co-sensitization," *Journal of Molecular Structure*, vol. 1206, article 127694, 2020.

[15] Z. Zolkepli, A. Lim, P. Ekanayake, and K. Tennakoon, "Efficiency enhancement of cocktail dye of Ixora coccinea and Tradescantia spathacea in DSSC," *Biophysics*, vol. 2015, article 582091, pp. 1–8, 2015.

[16] A. Dumbrava, J. Lungu, and A. Ion, "Green seaweeds extract as co-sensitizer for dye sensitized solar cells," *Chemical Engineering, Food Industry*, vol. 17, no. 1, p. 13, 2016.

[17] M. J. García-Salinas and M. J. Ariza, "Optimizing a simple natural dye production method for dye-sensitized solar cells: examples for betalain (bougainvillea and beetroot extracts) and anthocyanin dyes," *Applied Sciences*, vol. 9, no. 12, p. 2515, 2019.

[18] S. Sreeja and B. Pesala, "Performance enhancement of betanin solar cells co-sensitized with indigo and lawsone: a comparative study," *ACS Omega*, vol. 4, no. 19, pp. 18023–18034, 2019.

[19] A. Orona-Navar, I. Aguilar-Hernández, T. López-Luke et al., "Photoconversion efficiency of Titania solar cells co-sensitized with natural pigments from cochineal, papaya peel and microalga *Scenedesmus obliquus*," *Journal of Photochemistry and Photobiology A: Chemistry*, vol. 388, article 112216, 2020.

[20] J. M. Cole, G. Pepe, O. K. Al Bahri, and C. B. Cooper, "Cosensitization in dye-sensitized solar cells," *Chemical reviews*, vol. 119, no. 12, pp. 7279–7327, 2019.

[21] D. Colonna, V. Capogna, A. Lembo, T. M. Brown, A. Reale, and A. Di Carlo, "Efficient cosensitization strategy for dye-sensitized solar cells," *Applied Physics Express*, vol. 5, no. 2, article 022303, 2012.

[22] M. Cheng, X. Yang, J. Li, F. Zhang, and L. J. C. Sun, "Co-sensitization of organic dyes for efficient dye-sensitized solar," *ChemSusChem*, vol. 6, no. 1, pp. 70–77, 2013.

[23] S. Fan, X. Lu, H. Sun, G. Zhou, Y. J. Chang, and Z.-S. J. P. C. C. P. Wang, "Effect of the co-sensitization sequence on the performance of dye-sensitized solar cells with porphyrin and organic dyes," *Physical Chemistry Chemical Physics*, vol. 18, no. 2, pp. 932–938, 2016.

[24] M. Hosseinnezhad, S. Rouhani, and K. Gharanjig, "Extraction and application of natural pigments for fabrication of green dye-sensitized solar cells," *Opto-electronics review*, vol. 26, no. 2, pp. 165–171, 2018.

[25] F. Inakazu, Y. Noma, Y. Ogomi, and S. Hayase, "Dye-sensitized solar cells consisting of dye-bilayer structure stained with two dyes for harvesting light of wide range of wavelength," *Applied Physics Letters*, vol. 93, no. 9, p. 323, 2008.

[26] K. Lee, S. W. Park, M. J. Ko, K. Kim, and N. G. Park, "Selective positioning of organic dyes in a mesoporous inorganic oxide film," *Nature materials*, vol. 8, no. 8, pp. 665–671, 2009.

[27] S. W. Park, K. Lee, D.-K. Lee, M. J. Ko, N.-G. Park, and K. Kim, "Expanding the spectral response of a dye-sensitized solar cell by applying a selective positioning method," *Nanotechnology*, vol. 22, no. 4, article 045201, 2011.

[28] P. J. Holliman, K. J. Al-Salihi, A. Connell, M. L. Davies, E. W. Jones, and D. A. Worsley, "Development of selective, ultrafast multiple co-sensitization to control dye loading in dye-sensitized solar cells," *RSC advances*, vol. 4, no. 5, pp. 2515–2522, 2014.

[29] H.-J. Koo, K. Kim, N.-G. Park, S. Hwang, C. Park, and C. J. A. P. L. Kim, "Fabrication of heterosensitizer-junction dye-sensitized solar cells," *Applied Physics Letters*, vol. 92, no. 14, article 142103, 2008.

[30] S. Q. Fan, C. Kim, B. Fang et al., "Improved efficiency of over 10% in dye-sensitized solar cells with a ruthenium complex and an organic dye heterogeneously positioning on a single TiO2 electrode," *The Journal of Physical Chemistry C*, vol. 115, no. 15, pp. 7747–7754, 2011.

[31] C.-H. Yang, P.-Y. Chen, W.-J. Chen, T.-L. Wang, and Y.-T. J. E. A. Shieh, "Spectroscopic evidences of synergistic co-sensitization in dye-sensitized solar cells via experimentation of mixture design," *Electrochimica Acta*, vol. 107, pp. 170–177, 2013.

[32] S. Chang, H. Wang, Y. Hua et al., "Conformational engineering of co-sensitizers to retard back charge transfer for high-efficiency dye-sensitized solar cells," *Journal of Materials Chemistry A*, vol. 1, no. 38, pp. 11553–11558, 2013.

[33] A. K. Chandiran, N. Tetreault, R. Humphry-Baker et al., "Subnanometer Ga2O3 tunnelling layer by atomic layer deposition to achieve 1.1 V open-circuit potential in dye-sensitized solar cells," *Nano Letters*, vol. 12, no. 8, pp. 3941–3947, 2012.

[34] K. Hanson, M. D. Losego, B. Kalanyan, D. L. Ashford, G. N. Parsons, and T. J. Meyer, "Stabilization of $[Ru(bpy)_2(4,4'\text{-}(PO_3H_2)bpy)]^{2+}$ on Mesoporous TiO2 with Atomic Layer Deposition of Al2O3," *Chemistry of Materials*, vol. 25, no. 1, pp. 3–5, 2013.

[35] P. J. Holliman, M. Mohsen, A. Connell et al., "Ultra-fast co-sensitization and tri-sensitization of dye-sensitized solar cells with N719, SQ1 and triarylamine dyes," *Journal of Materials Chemistry A*, vol. 22, no. 26, pp. 13318–13327, 2012.

[36] N. T. Kumara, M. R. Kooh, A. Lim et al., "DFT/TDDFT and experimental studies of natural pigments extracted from black tea waste for DSSC application," *International Journal of Photoenergy*, vol. 2013, Article ID 109843, 8 pages, 2013.

[37] B. P. Kafle, B. R. Pokhrel, R. Gyawali et al., "Absorbance of natural and synthetic dyes: prospect of application as

sensitizers in dye sensitized solar cell," *cell*, vol. 5, no. 1, pp. 8–12, 2014.

[38] D. Pratiwi, F. Nurosyid, A. Supriyanto, and R. Suryana, "Efficiency enhancement of dye-sensitized solar cells (DSSC) by addition of synthetic dye into natural dye (anthocyanin)," in , Article ID 012012*IOP Conference Series: Materials Science and Engineering*, vol. 176, Surakarta, Indonesia, 2016.

[39] K. Zu, L. Zhang, and X. Sun, *Impact of co-sensitization of natural dyes anthocyanin and chlorophyll with N719 on dye-sensitized solar cells*, DEStech Transactions on Engineering and Technology Research amsm, 2017.

[40] G. Richhariya and A. J. O. M. Kumar, "Fabrication and characterization of mixed dye: natural and synthetic organic dye," *Optical Materials*, vol. 79, pp. 296–301, 2018.

[41] N. Madili, A. Pogrebnoi, and T. Pogrebnaya, *Theoretical design of complex molecule via combination of natural lawsone and synthetic indoline D131 dyes for dye sensitized solar cells application*, vol. 6, no. 4, 2018Scientific Research Publishing Inc., 2018.

[42] D. Pratiwi, F. Nurosyid, A. Supriyanto, and R. Suryana, "Effect of composition of chlorophyll and ruthenium dyes mixture (hybrid) on the dye-sensitized solar cell performance," in , Article ID 012030*IOP Conference Series: Materials Science and Engineering*, vol. 333, Surakarta, Indonesia, 2017.

[43] A. Msangi, A. Pogrebnoi, and T. Pogrebnaya, "Combination of natural dye (crocetin) and synthetic dye (indoline D205) for DSSCs application," *International Journal of Computational and Theoretical Chemistry*, vol. 6, no. 1, pp. 1–13, 2018.

[44] K. Ashok Kumar, J. Manonmani, and J. Senthilselvan, "Effect on interfacial charge transfer resistance by hybrid co-sensitization in DSSC applications," *Journal of Materials Science: Materials in Electronics*, vol. 25, no. 12, pp. 5296–5301, 2014.

[45] S. H. Cho and Y. J. Yoon, "Multi-layer $TiO_2$ films prepared by aerosol deposition method for dye-sensitized solar cells," *Thin Solid Films*, vol. 547, pp. 91–94, 2013.

[46] W. Wang, H. Yuan, J. Xie et al., "Enhanced efficiency of large-area dye-sensitized solar cells by light- scattering effect using multilayer $TiO_2$ photoanodes," *Materials Research Bulletin*, vol. 100, pp. 434–439, 2018.

[47] J. Xu, S. Wu, J. H. Ri, J. Jin, and T. Peng, "Bilayer film electrode of brookite $TiO_2$ particles with different morphology to improve the performance of pure brookite-based dye-sensitized solar cells," *Journal of Power Sources*, vol. 327, pp. 77–85, 2016.

[48] G. K. Senadeera, D. Balasundaram, M. A. Dissanayake et al., "Efficiency enhancement in dye-sensitized solar cells with co-sensitized, triple layered photoanode by enhanced light scattering and spectral responses," *Bulletin of Materials Science*, vol. 44, no. 1, pp. 1–8, 2021.

[49] N. I. Beedri, P. K. Baviskar, V. P. Bhalekar et al., "N3-sensitized $TiO_2/Nb_2O_5$: a novel bilayer structure for dye-sensitized solar-cell application," *Physica status solidi (a)*, vol. 215, no. 18, article 1800236, 2018.

[50] K. A. Bhatti, M. I. Khan, M. Saleem, F. Alvi, R. Raza, and S. Rehman, "Analysis of multilayer based TiO2 and ZnO photoanodes for dye-sensitized solar cells," *Materials Research Express*, vol. 6, no. 7, article 075902, 2019.

[51] S. Datta, A. Dey, N. R. Singha, and S. Roy, "Enhanced performance of dye-sensitized solar cell with thermally stable natural dye-assisted TiO2/MnO2 bilayer-assembled photoanode," *Materials for Renewable and Sustainable Energy*, vol. 9, no. 4, pp. 1–11, 2020.

[52] A. U. Rehman, M. Aslam, I. Shahid et al., "Enhancing the light absorption in dye-sensitized solar cell by using bilayer composite materials based photo-anode," *Optics Communications*, vol. 477, article 126353, 2020.

[53] S. W. Himmah, M. Diantoro, N. A. Astarini, S. K. G. Tiana, A. Hidayat, and A. Taufiq, "Structural, morphological, optical, and electrical properties of $TiO_2$/ZnO rods multilayer films as photoanode on dye-sensitized solar cells," in *Journal of Physics: Conference Series*, vol. 1816, Mataram, West Nusa Tenggara, Indonesia, 2021.

[54] J. W. Lee and J. H. Moon, "Monolithic multiscale bilayer inverse opal electrodes for dye-sensitized solar cell applications," *Nanoscale*, vol. 7, no. 12, pp. 5164–5168, 2015.

[55] A. Hidayat, A. Taufiq, Z. A. Supardi et al., "Synthesis and characterization of $TiO_2$/ZnO-Ag@ TiO2 nanocomposite and their performance as photoanode of organic dye-sensitized solar cell," *Materials Today: Proceedings*, vol. 44, pp. 3395–3399, 2021.

[56] Z. U. Rehman, S. Ali, M. Aslam et al., "Optical absorption modeling of bilayer photoanode based on Cu@ $TiO_2$ plasmonic dye sensitized solar cells towards photovoltaic applications," *Optical and Quantum Electronics*, vol. 53, no. 7, pp. 1–13, 2021.

[57] H. Chang, H. T. Su, W. A. Chen et al., "Fabrication of multilayer $TiO_2$ thin films for dye-sensitized solar cells with high conversion efficiency by electrophoresis deposition," *Solar Energy*, vol. 84, no. 1, pp. 130–136, 2010.

[58] A. Atli, A. Atilgan, and A. Yildiz, "Multi-layered $TiO_2$ photoanodes from different precursors of nanocrystals for dye-sensitized solar cells," *Solar Energy*, vol. 173, pp. 752–758, 2018.

[59] G. Fu, E. J. Cho, X. Luo et al., "Enhanced light harvesting in panchromatic double dye-sensitized solar cells incorporated with bilayered $TiO_2$ thin film-based photoelectrodes," *Solar Energy*, vol. 218, pp. 346–353, 2021.

[60] J. M. Cole, Y. Gong, J. McCree-Grey, P. J. Evans, and S. A. Holt, "Modulation of N3 and N719 dye···$TiO_2$ Interfacial Structures in Dye-Sensitized Solar Cells As Influenced by Dye Counter Ions, Dye Deprotonation Levels, and Sensitizing Solvent," *ACS Applied Energy Materials*, vol. 1, no. 6, pp. 2821–2831, 2018.

[61] H. Cheema, J. Watson, A. Peddapuram, and J. H. J. C. C. Delcamp, "A 25 mA $cm^{-2}$ dye-sensitized solar cell based on a near-infrared-absorbing organic dye and application of the device in SSM-DSCs," *Chemical Communications*, vol. 56, no. 11, pp. 1741–1744, 2020.

[62] L. Zhang, J. M. Cole, and C. Dai, "Variation in optoelectronic properties of azo dye-sensitized $TiO_2$ semiconductor interfaces with different adsorption anchors: carboxylate, sulfonate, hydroxyl and pyridyl groups," *ACS applied materials & interfaces*, vol. 6, no. 10, pp. 7535–7546, 2014.

[63] L. Zhang and J. M. Cole, "Anchoring groups for dye-sensitized solar cells," *ACS applied materials & interfaces*, vol. 7, no. 6, pp. 3427–3455, 2015.

[64] S. Feng, Z. Z. Sun, and Q. Li, "How to screen a promising anchoring group from heterocyclic components in dye sensitized solar cell: a theoretical investigation," *Electrochimica Acta*, vol. 296, pp. 545–554, 2019.

[65] A. Karakas, Y. Ceylan, M. Karakaya et al., "One-photon absorption characterizations, dipole polarizabilities and second hyperpolarizabilities of chlorophyll a and crocin," *Open Chemistry*, vol. 16, no. 1, pp. 1242–1247, 2018.

[66] S. A. Kandjani, S. W. Chan, R. Barille, S. Dabos-Seignon, and J. Nunzi, "Linear and nonlinear holographic gratings in Saffron," *Nonlinear Optics Quantum Optics*, vol. 36, no. 3/4, p. 195, 2007.

[67] L. J. Rather and F. Mohammad, "*Acacia nilotica* (L.): a review of its traditional uses, phytochemistry, and pharmacology," *Sustainable Chemistry and Pharmacy*, vol. 2, pp. 12–30, 2015.

[68] W. Wang, Y. Wu, H. Xu et al., "Accumulation mechanism of indigo and indirubin in *Polygonum tinctorium* revealed by metabolite and transcriptome analysis," *Industrial Crops and Products*, vol. 141, article 111783, 2019.

[69] D. Mammen and M. J. F. C. Daniel, "A critical evaluation on the reliability of two aluminum chloride chelation methods for quantification of flavonoids," *Food Chemistry*, vol. 135, no. 3, pp. 1365–1368, 2012.

[70] P. Trihutomo, S. Soeparman, D. Widhiyanuriyawan, and L. Yuliati, "Performance improvement of dye-sensitized solar cell- (DSSC-) based natural dyes by clathrin protein," *International Journal of Photoenergy*, vol. 2019, Article ID 4384728, 9 pages, 2019.

[71] A. A. Javidparvar, R. Naderi, B. Ramezanzadeh, and G. Bahlakeh, "Graphene oxide as a pH-sensitive carrier for targeted delivery of eco-friendly corrosion inhibitors in chloride solution: experimental and theroretical investigations," *Journal of industrial and engineering chemistry*, vol. 72, pp. 196–213, 2019.

[72] R. V. Lakshmi, G. Yoganandan, K. T. Kavya, and B. J. Basu, "Effective corrosion inhibition performance of $Ce^{3+}$ doped sol–gel nanocomposite coating on aluminum alloy," *Progress in Organic Coatings*, vol. 76, no. 2-3, pp. 367–374, 2013.

[73] A. B. Nandiyanto, R. Oktiani, and R. Ragadhita, "How to read and interpret FTIR spectroscope of organic material," *Indonesian Journal of Science and Technology*, vol. 4, no. 1, pp. 97–118, 2019.

[74] C. G. Anchieta, A. Cancelier, M. A. Mazutti et al., "Effects of solvent diols on the synthesis of $ZnFe_2O_4$ particles and their use as heterogeneous photo-Fenton catalysts," *Materials*, vol. 7, no. 9, pp. 6281–6290, 2014.

[75] J. Coates, *Interpretation of Infrared Spectra, A Practical Approach*, Citeseer, 2000.

[76] M. R. Jung, F. D. Horgen, S. V. Orski et al., "Validation of ATR FT-IR to identify polymers of plastic marine debris, including those ingested by marine organisms," *Marine Pollution Bulletin*, vol. 127, pp. 704–716, 2018.

[77] K. Fischer, A. Gawel, D. Rosen et al., "Low-temperature synthesis of anatase/rutile/brookite TiO2 nanoparticles on a polymer membrane for photocatalysis," *Catalysts*, vol. 7, no. 7, p. 209, 2017.

[78] S. Yin, H. Hasegawa, D. Maeda, M. Ishitsuka, and T. Sato, "Synthesis of visible-light-active nanosize rutile titania photocatalyst by low temperature dissolution–reprecipitation process," *Journal of Photochemistry and Photobiology A: Chemistry*, vol. 163, no. 1-2, pp. 1–8, 2004.

[79] Z. Yanqing, S. Erwei, C. Zhizhan, L. Wenjun, and H. Xingfang, "Influence of solution concentration on the hydrothermal preparation of titania crystallites," *Journal of materials Chemistry*, vol. 11, no. 5, pp. 1547–1551, 2001.

[80] M. Wu, G. Lin, D. Chen et al., "Sol-hydrothermal synthesis and hydrothermally structural evolution of nanocrystal titanium dioxide," *Chemistry of Materials*, vol. 14, no. 5, pp. 1974–1980, 2002.

[81] Z. Zhong, T. P. Ang, J. Luo, H. C. Gan, and A. Gedanken, "Synthesis of one-dimensional and porous $TiO_2$ nanostructures by controlled hydrolysis of titanium alkoxide via coupling with an esterification reaction," *Chemistry of materials*, vol. 17, no. 26, pp. 6814–6818, 2005.

[82] M. R. Karim, M. T. Bhuiyan, M. A. Dar et al., "Synthesis and characterization of highly organized crystalline rutile nanoparticles by low-temperature dissolution-reprecipitation process," *Journal of Materials Research*, vol. 30, no. 12, pp. 1887–1893, 2015.

[83] A. G. Gaynor, R. J. Gonzalez, R. M. Davis, and R. Zallen, "Characterization of nanophase titania particles synthesized using *in situ* steric stabilization," *Journal of materials research*, vol. 12, no. 7, pp. 1755–1765, 1997.

[84] P. J. G. W. G. Scherrer, *Bestimmung der Grösse und der inneren von Kolloidteilchen mittels Röntgenstrahlen Struktur Nachr*, vol. 26, Springer, 1918.

[85] J. C. Chou, C. H. Huang, Y. H. Liao, Y. J. Lin, C. M. Chu, and Y. H. Nien, "Analysis of different series-parallel connection modules for dye-sensitized solar cell by electrochemical impedance spectroscopy," *International Journal of Photoenergy*, vol. 2016, Article ID 6595639, 8 pages, 2016.

[86] A. Sacco, "Electrochemical impedance spectroscopy: fundamentals and application in dye-sensitized solar cells," *Renewable and Sustainable Energy Reviews*, vol. 79, pp. 814–829, 2017.

[87] D. Zhao, T. Peng, L. Lu, P. Cai, P. Jiang, and Z. Bian, "Effect of annealing temperature on the photoelectrochemical properties of dye-sensitized solar cells made with mesoporous $TiO_2$ nanoparticles," *The Journal of Physical Chemistry C*, vol. 112, no. 22, pp. 8486–8494, 2008.

[88] H. K. Sung, Y. Lee, W. H. Kim et al., "Enhanced power conversion efficiency of dye-sensitized solar cells by band edge shift of $TiO_2$ photoanode," *Molecules*, vol. 25, no. 7, p. 1502, 2020.

[89] A. C. Santulli, C. Koenigsmann, A. L. Tiano, D. DeRosa, and S. S. J. N. Wong, "Correlating titania morphology and chemical composition with dye-sensitized solar cell performance," *Nanotechnology*, vol. 22, no. 24, article 245402, 2011.

[90] M. Jankulovska, T. Berger, S. S. Wong, R. Gómez, and T. Lana-Villarreal, "Trap states in $TiO_2$ films made of nanowires, nanotubes or nanoparticles: an electrochemical study," *ChemPhysChem*, vol. 13, no. 12, pp. 3008–3017, 2012.

[91] B. A. Kumar, G. Ramalingam, D. Karthigaimuthu, T. Elangovan, and V. Vetrivelan, "Fabrication of natural dye sensitized solar cell using tridax procumbens leaf and beetroot extract mixer as a sensitizer," *Materials Today: Proceedings*, vol. 49, pp. 2541–2545, 2022.

[92] S. Shah, M. H. Buraidah, L. P. Teo, M. A. Careem, and A. K. Arof, "Dye-sensitized solar cells with sequentially deposited anthocyanin and chlorophyll dye as sensitizers," *Optical and Quantum Electronics*, vol. 48, no. 3, pp. 1–8, 2016.

[93] C. Gautam, A. Singh, S. W. Gosavi et al., "Ferrocenyl-2-pyridylimine derived $d^{10}$-configuration complexes as prospective co-sensitizers in dye sensitized solar cells (DSSCs)," *Applied Organometallic Chemistry*, vol. 36, no. 4, 2022.

[94] T. H. Lwin, S. S. Than, S. H. Aung, N. W. Lwin, T. Z. Oo, and F. Chen, "The improved photocurrent density of D35-cpdt and DN-F10 via co-sensitization process in dye-sensitized solar cells," *Ionics*, vol. 28, no. 3, pp. 1461–1471, 2022.

[95] N. Ruba, S. Sowmaya, P. Prakash, B. Janarthanan, and P. A. Nagamani, "Dye-sensitized solar cells using a cocktail of synthetic (eosin Y) and natural (beetroot, pomegranate, and kumkum) dyes," *Brazilian Journal of Physics*, vol. 51, no. 5, pp. 1459–1465, 2021.

[96] D. N. Liyanage, K. D. Kumarasinghe, G. R. Kumara, A. C. Jayasundera, K. Tennakone, and B. Onwona-Agyeman, "Donor-$\pi$-conjugated spacer-acceptor dye-sensitized solid-state solar cell using CuI as the hole collector," *International Journal of Photoenergy*, vol. 2019, Article ID 1653027, 5 pages, 2019.

[97] H. C. Weerasinghe, P. M. Sirimanne, G. V. Franks, G. P. Simon, and Y. B. Cheng, "Low temperature chemically sintered nano-crystalline $TiO_2$ electrodes for flexible dye-sensitized solar cells," *Journal of Photochemistry and Photobiology A: Chemistry*, vol. 213, no. 1, pp. 30–36, 2010.

[98] M. Mojiri-Foroushani, H. Dehghani, and N. Salehi-Vanani, "Enhancement of dye-sensitized solar cells performances by improving electron density in conduction band of nanostructure $TiO_2$ electrode with using a metalloporphyrin as additional dye," *Electrochimica Acta*, vol. 92, pp. 315–322, 2013.

[99] A. Okello, B. O. Owuor, J. Namukobe, D. Okello, and J. Mwabora, "Influence of concentration of anthocyanins on electron transport in dye sensitized solar cells," *Heliyon*, vol. 7, no. 3, article e06571, 2021.

[100] E. Maggio, N. Martsinovich, and A. Troisi, "Evaluating charge recombination rate in dye-sensitized solar cells from electronic structure calculations," *Physical Chemistry C*, vol. 116, no. 14, pp. 7638–7649, 2012.

[101] T. Hannappel, B. Burfeindt, W. Storck, and F. Willig, "Measurement of ultrafast photoinduced electron transfer from chemically anchored Ru-dye molecules into empty electronic states in a colloidal anatase $TiO_2$ film," *Physical Chemistry B*, vol. 101, no. 35, pp. 6799–6802, 1997.

[102] M. Yanagida, Y. Numata, K. Yoshimatsu, S. Satoh, and L. Han, "Effective charge collection in dye-sensitized nanocrystalline $TiO_2$," *Advances in Natural Sciences: Nanoscience and Nanotechnology*, vol. 4, no. 1, article 015006, 2013.

[103] L. Y. Lin, C. P. Lee, K. W. Tsai et al., "Low-temperature flexible Ti/$TiO_2$ photoanode for dye-sensitized solar cells with binder-free $TiO_2$ paste," *Progress in Photovoltaics: Research*, vol. 20, no. 2, pp. 181–190, 2012.